Phospholipase Cγ2 regulates endocannabinoid and eicosanoid networks in innate immune cells

Hui Jing[a], Alex Reed[a], Olesya A. Ulanovskaya[b], Jan-Sebastian Grigoleit[b], Dylan M. Herbst[b], Cassandra L. Henry[b], Haoxin Li[a], Sabrina Barbas[a], Jason Germain[a], Kim Masuda[a], and Benjamin F. Cravatt[a,1]

[a]Department of Chemistry, The Scripps Research Institute, La Jolla, CA 92037; and [b]Lundbeck La Jolla Research Center, La Jolla, CA 92121

Contributed by Benjamin F. Cravatt, August 19, 2021 (sent for review July 14, 2021; reviewed by Jeremy M. Baskin and Michael Best)

Human genetic studies have pointed to a prominent role for innate immunity and lipid pathways in immunological and neurodegenerative disorders. Our understanding of the composition and function of immunomodulatory lipid networks in innate immune cells, however, remains incomplete. Here, we show that phospholipase Cγ2 (PLCγ2 or PLCG2)—mutations in which are associated with autoinflammatory disorders and Alzheimer's disease—serves as a principal source of diacylglycerol (DAG) pools that are converted into a cascade of bioactive endocannabinoid and eicosanoid lipids by DAG lipase (DAGL) and monoacylglycerol lipase (MGLL) enzymes in innate immune cells. We show that this lipid network is tonically stimulated by disease-relevant human mutations in PLCγ2, as well as Fc receptor activation in primary human and mouse macrophages. Genetic disruption of PLCγ2 in mouse microglia suppressed DAGL/MGLL-mediated endocannabinoid-eicosanoid cross-talk and also caused widespread transcriptional and proteomic changes, including the reorganization of immune-relevant lipid pathways reflected in reductions in DAGLB and elevations in PLA2G4A. Despite these changes, *Plcg2*$^{-/-}$ mice showed generally normal proinflammatory cytokine and chemokine responses to lipopolysaccharide treatment, instead displaying a more restricted deficit in microglial activation that included impairments in prostaglandin production and CD68 expression. Our findings enhance the understanding of PLCγ2 function in innate immune cells, delineating a role in cross-talk with endocannabinoid/eicosanoid pathways and modulation of subsets of cellular responses to inflammatory stimuli.

phospholipase | endocannabinoid | immune | nervous system | eicosanoid

Lipids function as components of cell membranes, sources of energy storage, and as chemical messengers that modulate diverse physiological processes. The central role of lipids in human biology has been underscored by the discovery of numerous disease-relevant mutations in lipid metabolic enzymes (1–5), transporters (6–8), and receptors (9, 10).

Among bioactive lipids, those possessing C20:4 (or arachidonoyl) acyl chains frequently serve as transmitters [e.g., endocannabinoids (11)] or substrates for oxidative reactions to furnish diverse classes of signaling molecules [e.g., eicosanoids (12, 13)]. The nervous and immune systems, as well as the cross-talk between them, appear to be particularly sensitive to the genetic or pharmacological perturbation of metabolic and signaling pathways that utilize C20:4 lipids. Eicosanoids, such as the prostaglandins and leukotrienes, for example, modulate inflammatory and nociceptive responses, and drugs targeting the enzymes that produce—or receptors that bind—eicosanoids are mainstay therapies for treating pain, asthma, and other disorders (12, 14). Endocannabinoid enzymes and receptors are likewise the targets of candidate therapeutics for a range of immunological and nervous system disorders (11, 15).

Recent human genetic studies further underscore the immunological and neurological relevance of the enzymatic pathways that incorporate, remodel, and release C20:4 acyl groups from phospholipids. For example, deleterious mutations in MBOAT7, the principal acyltransferase responsible for incorporating C20:4 fatty acids into phosphatidylinositol (PI) lipids (Fig. 1*A*), cause a human neurological disorder that manifests in mental retardation and propensity for seizures (2). Likewise, mutations in phospholipase C enzymes, which catalyze the hydrolysis of phosphatidyl-1D-myo-inositol 4,5-bisphosphate (PIP_2) to furnish the endocannabinoid/eicosanoid precursor C20:4 diacylglycerol (DAG) and myo-inositol 1,4,5-trisphosphate (IP_3) (Fig. 1*A*), produce a range of immunological and neurological diseases in humans (16–18). One striking example is phospholipase Cγ2 (PLCγ2, or PLCG2), which is predominantly expressed in hematopoietic cells in the periphery (19) and microglia in the central nervous system (CNS) (10, 20). Germline deletion of exons 19 or 20 to 22 in the *PLCG2* gene leads to cold urticaria and PLCγ2-associated antibody deficiency and immune dysregulation (PLAID) (21), while an activating missense mutation (S707Y or L848P) causes autoinflammatory PLAID (APLAID) (22, 23). *PLCG2* mutations have also been found in association with childhood-onset steroid-sensitive nephrotic syndrome (24), endemic Burkitt lymphoma (25), BTK inhibitor-resistant chronic lymphoma leukemia (CLL) (26, 27), and azacitidine and lenalidomide therapy-resistant high-risk myelodysplastic syndromes (28). Most recently, a rare P522R missense variant that modestly potentiates PLCγ2 activity has been found to be protective for late-onset Alzheimer's disease (LOAD), pointing to a provocative association between PLCγ2 function and AD pathogenesis (10, 20, 29). Also consistent with contributions of PLCγ2 to neuroimmunological signaling pathways, this enzyme was

Significance

Here, we reveal that activation of phospholipase Cγ2 (PLCγ2) by disease-relevant mutations or Fc receptor signaling stimulates the production of the endocannabinoid 2-arachidonylglycerol and prostaglandins in primary human and mouse immune cells through a pathway that involves the DAG lipase (DAGL) and monoacylglycerol lipase (MGLL) enzymes. *Plcg2* deficiency suppressed DAGL/MGLL-mediated endocannabinoid-eicosanoid cross-talk in mouse microglia, leading to impairment in lipopolysaccharide-mediated microglia activation in vivo that included reduced prostaglandin production and CD68 expression. Our studies provide important mechanistic insights into the regulation of lipid signaling pathways in primary immune cells, revealing a PLCγ2-DAGL-MGLL network that may serve as a future target for treating diverse immunopathologies.

Author contributions: H.J., O.A.U., and B.F.C. designed research; H.J., A.R., J.-S.G., D.M.H., C.L.H., S.B., J.G., and K.M. performed research; H.J. contributed new reagents/analytic tools; H.J., O.A.U., H.L., and B.F.C. analyzed data; and H.J., A.R., O.A.U., and B.F.C. wrote the paper.

Reviewers: J.M.B., Cornell University; M.B., University of Tennessee Knoxville.

The authors declare no competing interest.

[1]To whom correspondence may be addressed. Email: cravatt@scripps.edu.

This article contains supporting information online at https://www.pnas.org/lookup/suppl/doi:10.1073/pnas.2112971118/-/DCSupplemental.

Published October 4, 2021.

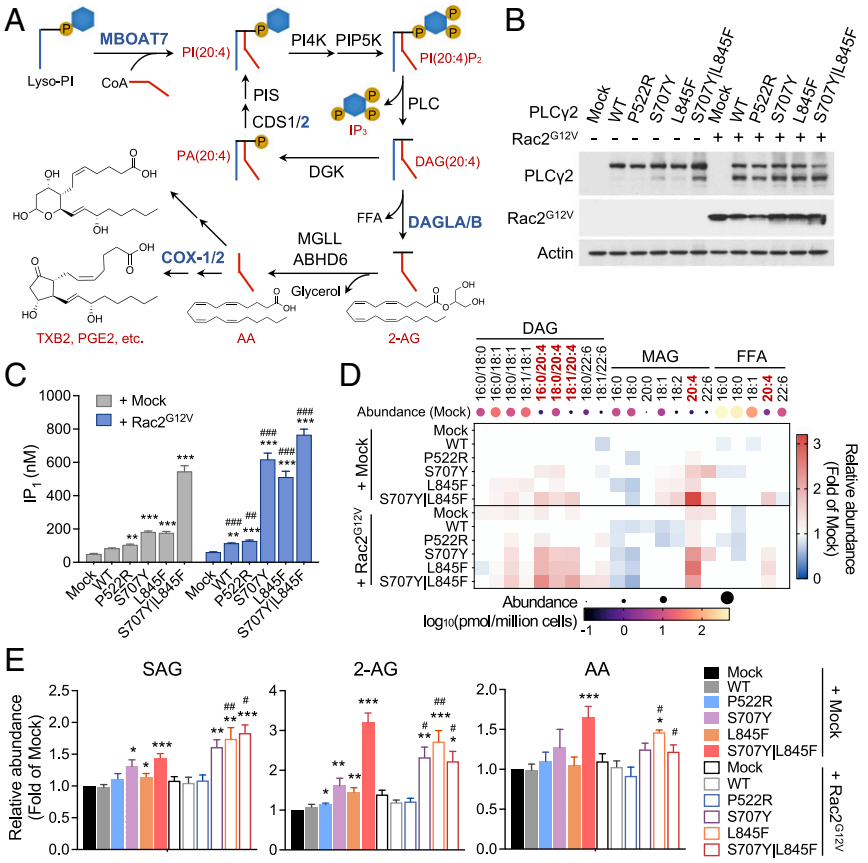

Fig. 1. Hyperactivating PLCγ2 variants stimulate endocannabinoid production in HEK293T cells. (*A*) Schematic of a C20:4 lipid network leading to endocannabinoid (2-AG) and eicosanoid production. Highlighted in blue are the enzymes with C20:4 lipid substrate preference. (*B*) Representative anti-FLAG immunoblots showing expression of PLCγ2_WT and indicated PLCγ2 variants, as well as $Rac2^{G12V}$, in HEK293T cells. (*C*) Effects of PLCγ2_WT and PLCγ2 variants on IP_1 (surrogate for IP_3) content with or without $Rac2^{G12V}$ coexpression in HEK293T cells. Data represent mean values ± SEM from three biologically independent experiments. (*D*) Heatmap showing relative DAG, MAG, and FFA content in HEK293T cells expressing PLCγ2_WT or the indicated PLCγ2 variants, with or without $Rac2^{G12V}$ coexpression. Values are normalized to Mock-transfected cells set to a value of 1 and values for groups with $P > 0.05$ vs. Mock-transfected cells are indicated as 1 on heatmap. Absolute abundance of indicated lipid species in the Mock-transfected cells is shown with bubble plot above the heatmap. (*E*) Bar graphs showing changes in SAG, 2-AG, and AA content in *D*. For *D* and *E*, data represent mean values ± SEM from six biologically independent experiments. Statistical significance was calculated with two-tailed Student's *t* tests; $^{*}P < 0.05$, $^{**}P < 0.01$, $^{***}P < 0.001$ for PLCγ2_WT/variants- vs. Mock-transfected cells; and $^{\#}P < 0.05$, $^{\#\#}P < 0.01$, $^{\#\#\#}P < 0.001$, for Mock- vs. $Rac2^{G12V}$-transfected cells.

recently found to contribute to downstream signaling from TREM2 (30), a surface receptor that also shows strong human genetic links to AD (10, 31).

Despite generating two key second messengers, IP_3 and DAG, the latter of which also serves as metabolic source for the endocannabinoid 2-arachidonoylglycerol (2-AG) and downstream prostaglandins, the impact of PLCγ2 activation on C20:4 lipid signaling pathways remains poorly understood. Prompted by the human genetics link between PLCγ2 and immune and neurological disorders, as well as the key roles that endocannabinoids and eicosanoids play in neuroimmunology, we herein describe the mechanistic characterization of functional cross-talk between PLCγ2 and endocannabinoid/eicosanoid pathways in primary human and mouse innate immune cells. Our results reveal that activation of PLCγ2 by genetic mutation or upstream Fcγ receptor (FcγR) cross-linking leads to elevated flux through a C20:4 DAG-2-AG-arachidonic acid (AA)-prostaglandin pathway involving the diacylglycerol lipase (DAGL) and monoacylglycerol lipase (MGLL) enzymes. We further show that genetic inactivation of PLCγ2 impairs lipopolysaccharide (LPS)-induced microglial activation and prostaglandin formation in mice while sparing bulk endocannabinoids, pointing to a specialized role for PLCγ2 in generating immune-relevant bioactive lipids in the CNS.

Results

Hyperactivating PLCγ2 Variants Stimulate a DAG-2-AG-AA Lipid Network. Considering the immune cell-restricted expression profile and minimal enzymatic activity of PLCγ2 in its basal autoinhibited state (22, 32, 33), we first sought to investigate the impact of PLCγ2 activation on the DAG-2-AG-AA pathway by expressing gain-of-function PLCγ2 variants in a nonimmune cell model system. We selected three previously characterized disease-relevant hypermorphic PLCγ2 variants—P522R, S707Y, and L845F—for analysis in HEK293T cells. These mutations have been associated with different human pathological phenotypes and have varying effects on basal PLCγ2 activity. For example, PLCγ2_P522R, which has been reported to weakly stimulate PLCγ2 catalytic activity (20) and promote beneficial microglial function (34), has been linked to protection against LOAD (10). PLCγ2_S707Y, which, in germline form, gives rise to APLAID (22) and is somatically found in ibrutinib-resistant CLL (27, 32), promotes robust activation of the enzyme (22, 32), as does PLCγ2_L845F, which is also associated with ibrutinib-resistance in CLL patients (35). The S707Y and L845F mutations can furthermore co-occur in some ibrutinib-resistant CLL patients (26, 36) and synergize to enhance the basal activity of PLCγ2 (32). We therefore included a PLCγ2 variant with the

S707Y|L845F double mutation in our studies. Consistent with past studies (32), recombinant expression of PLCγ2_S707Y and _L845F significantly increased IP_1 content of HEK293T cells [IP_1 is used as a surrogate measurement for IP_3 (37)], with the S707Y|L845F double mutant demonstrating an even greater activity (Fig. 1 *B* and *C* and *SI Appendix*, Fig. S1 *A* and *B*).

In contrast, expression of PLCγ2_WT or PLCγ2_P522R had limited impact on the basal quantity of IP_1 in HEK293T cells (Fig. 1 *B* and *C*). The PLCγ2_S707Y and _L845F variants have been shown to be further stimulated by interactions with the small GTPase Rac2 (32, 35), and we found that all PLCγ2 variants, as well as PLCγ2_WT, produced greater IP_1 elevations in HEK293T cells coexpressing a constitutively active $Rac2^{G12V}$ (Fig. 1 *B* and *C*). The expression level of $Rac2^{G12V}$ was consistently lower in the presence of WT-PLCγ2 or PLCγ2_P522R compared to other PLCγ2 mutants or even mock-transfected cells (Fig. 1*B* and *SI Appendix*, Fig. S1*B*). While we do not understand the reason for this difference in $Rac2^{G12V}$ expression, we observed similar relative IP_1 stimulatory activity for the PLCγ2 mutants in a second cell line COS-7, where $Rac2^{G12V}$ coexpression was unaffected (*SI Appendix*, Fig. S1 *C* and *D*). We also observed the presence of a lower molecular weight form of PLCγ2 in cells coexpressing $Rac2^{G12V}$, as well as constitutively for PLCγ2_S707Y|L845F (Fig. 1*B* and *SI Appendix*, Fig. S1 *A* and *C*). Whether this lower molecular weight PLCγ2, which was present in both transfected HEK293T cells and to a lesser extent in COS-7 cells, reflects proteolysis or another posttranslational modification, its general correlation with increased activity states for the PLCγ2 variants suggests that it may represent a functional proteoform of this phospholipase.

We next performed targeted lipidomic analysis of PLCγ2-expressing HEK293T cells using liquid-chromatography-mass spectrometry (MS), which revealed that the more activated PLCγ2 variants—S707Y, L845F, and S707|L845F—but not PLCγ2_WT or PLCγ2_P522R, elevated diverse unsaturated DAG and monoacylglycerol (MAG) lipids, most prominently C20:4-containing DAGs (C18:0/20:4- [SAG], C16:0/20:4- and C18:1/20:4-DAGs), and 2-AG (Fig. 1 *D* and *E* and *SI Appendix*, Fig. S1*E* and Dataset S1). For PLCγ2_S707|L845F, which displayed the strongest effects on C20:4-DAG and 2-AG, we additionally observed an increase in AA. Coexpression of $Rac2^{G12V}$ resulted in enhanced production of SAG, 2-AG, and AA by both PLCγ2_S707Y and PLCγ2_L845F, while having variable impact on PLCγ2_S707|L845F reflected in higher SAG, but paradoxically somewhat blunted increases in 2-AG and AA (Fig. 1 *D* and *E*). We do not understand why $Rac2^{G12V}$ coexpression suppressed the elevations in 2-AG and AA caused by PLCγ2_S707|L845F (Fig. 1 *D* and *E*), but this could reflect a rewiring of lipid networks caused by very high flux in the PIP_2-DAG-2-AG-AA pathway. Neither PLCγ2_WT nor PLCγ2_P522R produced substantial changes in SAG, 2-AG, or AA, regardless of coexpression with $Rac2^{G12V}$. In addition, we observed variable degrees of reduction of saturated C16:0- and C18:0-MAGs in cells expressing PLCγ2 (both WT and activating variants) with or without $Rac2^{G12V}$ coexpression (Fig. 1*D*), but these changes did not correlate with the profile of coordinated elevations in SAG, 2-AG, or AA. Taken together, these results indicate that disease-relevant activating

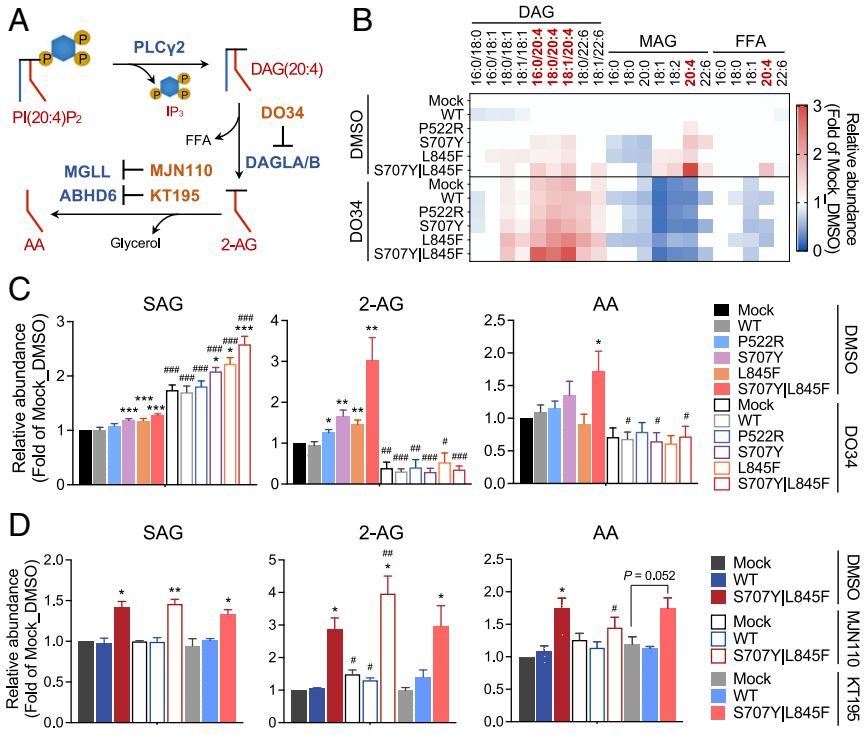

Fig. 2. Hyperactivating PLCγ2-mediated endocannabinoid production requires DAGL and MGLL in HEK293T cells. (*A*) Schematic of proposed DAGL/MGLL-dependent DAG-2-AG-AA flux downstream of PLCγ2. (*B*) Heatmap showing effect of DAGL inhibitor DO34 (100 nM, 4 h) on DAG, MAG, and FFA content in HEK293T cells expressing PLCγ2_WT or the indicated PLCγ2 variants. Values are normalized to Mock-transfected cells treated with DMSO set to a value of 1 and values for groups with $P > 0.05$ vs. Mock-transfected cells treated with DMSO are indicated as 1 on heatmap. (*C*) Bar graphs showing changes in SAG, 2-AG, and AA content in *B*. (*D*) Effects of MGLL inhibitor MJN110 (100 nM, 4 h) or ABHD6 inhibitor KT195 (100 nM, 4 h) on SAG, 2-AG, and AA content in HEK293T cells expressing PLCγ2_WT or hyperactivating variant PLCγ2_S707Y|L845F. For *B*–*D*, data represent mean values ± SEM normalized to DMSO-treated, Mock-transfected group, from three to six (*B* and *C*) or three to four (*D*) biologically independent experiments. Statistical tests: two-tailed Student's *t* tests. $^{*}P < 0.05$, $^{**}P < 0.01$, $^{***}P < 0.001$ for PLCγ2 WT/variants- vs. Mock-transfected cells; and $^{\#}P < 0.05$, $^{\#\#}P < 0.01$, $^{\#\#\#}P < 0.001$, for DO34, MJN110 or KT195- vs. DMSO-treated cells.

mutations in PLCγ2 promote constitutive DAG-2-AG-AA lipid flux in human cells that can also be further stimulated by $Rac2^{G12V}$.

DAGL and MGLL Enzymes Act Downstream of PLCγ2 in a DAG-2-AG-AA Lipid Network. Previous studies have demonstrated that DAGLs (DAGLA and DAGLB) and MGLL are major 2-AG biosynthetic and degradative enzymes, respectively (38–42). However, their connectivity to specific PLC enzymes has not been extensively investigated except in certain neuronal cell types (38). HEK293T cells expressing WT or activating variants of PLCγ2 were treated with the DAGL inhibitor DO34 (43) (100 nM, 4 h) (Fig. 2*A*), which led to elevations in C20:4 and other unsaturated DAGs and reduction in 2-AG and AA (Fig. 2 *B* and *C* and Dataset S1). Of note, DO34 further augmented the C20:4-containing DAGs, including SAG, increases caused by activating PLCγ2 variants—S707Y, L845, and S707|L845F—while completely blocking their stimulation of 2-AG and, in the case of PLCγ2_S707|L845F, AA production (Fig. 2*C* and *SI Appendix*, Fig. S2*A*). A similar lipid profile was observed for DO34-treated cells coexpressing PLCγ2 variants with $Rac2^{G12V}$ (*SI Appendix*, Fig. S2 *B* and *C* and Dataset S1). We next evaluated the contributions of 2-AG hydrolases MGLL and ABHD6 by treating cells with the inhibitors MJN110 (44) and KT195 (39), respectively (Fig. 2*A*). Since PLCγ2_S707|L845F produced the most robust increases in 2-AG and AA in HEK293T cells (Figs. 1*E* and 2*C*), we evaluated the effects of 2-AG hydrolase inhibitors (100 nM, 4 h) in HEK293T cells expressing PLCγ2_S707|L845F and found that the MGLL inhibitor MJN110, but not the ABHD6 inhibitor KT195, further augmented PLCγ2_S707|L845F-mediated elevation in 2-AG and inhibited the increase in AA without affecting SAG content (Fig. 2*D* and Dataset S1).

The results from HEK293T cells recombinantly expressing PLCγ2 variants revealed that activating mutations in this enzyme produce a tonic stimulation of the DAG-2-AG-AA pathway mediated, at least in part, by DAGL and MGLL enzymes. However, whether WT-PLCγ2 forms a functional network with DAGL and MGLL in more physiologically relevant (e.g., primary immune) cell types remained unknown. To address this important question, we first examined the expression of PLCγ2 and the related PLC isozyme, PLCγ1, in human peripheral blood mononuclear cells (hPBMCs) and monocyte-derived macrophages (hMDMs), as well as mouse bone marrow-derived macrophages (mBMDMs). Both PLCγ1 and PLCγ2 were expressed in hPBMCs, but only PLCγ2 was expressed in hMDMs or mBMDMs (Fig. 3*A*). We also examined hMDMs by activity-based protein profiling (ABPP) using the serine hydrolase-directed probe fluorophosphonate-biotin (FP-biotin) (45) and quantitative MS-based proteomics (46), which revealed strong expression of both DAGLB and MGLL (*SI Appendix*, Fig. S3*A*). DAGLA was not detected in hMDMs, consistent with its predominant expression in the nervous system (41). The expression of MGLL in hMDMs was interesting, as this enzyme is largely absent from commonly used mouse macrophages cell lines (e.g., RAW264.7 and J774 cells) (47, 48). Competitive ABPP further confirmed blockade of DAGLB activity in hMDMs by DO34 (100 nM, 4 h) (*SI Appendix*, Fig. S3*B*), while MGLL was inhibited, as expected, by MJN110 (100 nM, 4 h) (*SI Appendix*, Fig. S3*B*), but also partly by DO34 (*SI Appendix*, Fig. S3*B*). The cross-reactivity of human MGLL with DO34 was surprising, as it has not been observed for mouse MGLL in brain tissue from treated animals (43). Fortunately, a second DAGL inhibitor DH376 did not cross-react with human MGLL in hMDMs (*SI Appendix*, Fig. S3*C*). DO34 and DH376 more generally showed overlapping, but complementary off-target profiles across the serine hydrolase class (*SI Appendix*, Fig. S3 *B–D*), motivating us to utilize both compounds in our studies of DAGL contributions in hMDMs. Additionally, considering DO34, DH376, and MJN110 all cross-reacted with the alternative 2-AG hydrolase ABHD6 (*SI Appendix*, Fig. S3 *B* and *C*), as previously reported (43, 44), the selective ABHD6 inhibitor KT195 (39) was additionally tested in hMDMs.

Having established the presence of PLCγ2, DAGLB, and MGLL in hMDMs, we next sought to determine whether these enzymes organize into a functional metabolic/signaling pathway. As a means to activate PLCγ2, we incubated the hMDMs with human IgG followed by anti-IgG $F(ab')_2$ to form IgG immune complexes (IgG-IC) that cross-link FcγRs, which has been demonstrated to induce PLCγ2-dependent Ca^{2+} flux in mouse macrophages (19). FcγR cross-linking by IgG-IC increased the IP_1 content of hMDMs (Fig. 3*B*) and promoted the time-dependent phosphorylation of PLCγ2 at Tyr759 (Fig. 3*C* and *SI Appendix*, Fig. S4*A*), which is indicative of PLCγ2 activation (49). FcγR cross-linking also caused a temporally restricted elevation in SAG, 2-AG, and AA in hMDMs, which returned to basal levels 60 to 120 min after IgG-IC stimulation (Fig. 3*D*). Of note, while the magnitude of increase in SAG, 2-AG, and AA varied in hMDMs from donor to donor, the increase and its time-dependency were consistent across donors. Finally, despite observing an increase in AA following IgG-IC treatment, prostaglandins were paradoxically decreased (*SI Appendix*, Fig. S4*B*), suggesting that the IgG-IC–induced pool of AA is uncoupled from prostaglandin production.

Pretreatment with DO34 (100 nM, 3 h) or DH376 (1 μM, 3 h) prior to IgG-IC augmented SAG content of hMDMs under basal and stimulated conditions and blocked IgG-IC–induced elevation in 2-AG (Fig. 3*D* and *SI Appendix*, Fig. S4*C*). The IgG-IC–induced increases in AA were also partly suppressed by treatment with either DAGL inhibitor (Fig. 3*D* and *SI Appendix*, Fig. S4*C*). Pretreating hMDMs with MJN110 (100 nM, 3 h) produced a complementary lipid profile that included increases in basal and IgG-IC–induced 2-AG content alongside partial blockade of IgG-IC–induced increases in AA (Fig. 3*E*). Moreover, blockade of ABHD6 by KT195 (100 nM, 3 h) did not significantly impact basal SAG, 2-AG, or AA content in hMDMs (*SI Appendix*, Fig. S4*D*). These results therefore suggest that DAGL mediates DAG-to-2-AG and MGLL mediates 2-AG-to-AA flux upon FcγR cross-linking. Since DAGL acts upstream of MGLL, the effects of DO34 on DAG-2-AG-AA flux were similar to DH376 and not confounded by its cross-reactivity against MGLL (Fig. 3*D* and *SI Appendix*, Fig. S4*C*). Interestingly, pretreatment with MJN110 was found to also up-regulate SAG at 60 min after IgG-IC stimulation (Fig. 3*E*), which contrasted with the lack of effect of this MGLL inhibitor on SAG content in unstimulated hMDMs or in HEK293T cells overexpressing activating variants of PLCγ2 (Fig. 2*D*). We speculate that FcγR cross-linking, by increasing the flux of lipid metabolism through the PLCγ2-DAGL-MGLL pathway, may provide a specialized context where MGLL inhibition enables conversion of 2-AG back to SAG. Finally, in line with the effects of activating mutations in PLCγ2 studied in HEK293T cells (Fig. 1*D*), FcγR cross-linking caused elevation in other unsaturated DAG and MAG species in hMDMs, while saturated DAGs, MAGs, and most free fatty acids (FFAs) (with the exception of AA) were unchanged. DAGL and MGLL inhibitors impacted these additional DAG and MAG profiles similarly to the effects on C20:4 DAG and 2-AG (*SI Appendix*, Fig. S4 *E* and *F* and Dataset S1).

These results, taken together, support the presence of a PLCγ2-DAGL-MGLL pathway in hMDMs that is stimulated by FcγR cross-linking to promote flux through a DAG-2-AG-AA lipid signaling network.

PLCγ2-DAGL-MGLL Pathway in Mouse Macrophage and Microglia. We next acquired *Plcg2*$^{-/-}$ mice to study in more depth the PLCγ2 contributions to DAG-2-AG-AA lipid pathway flux in innate immune cells, specifically mouse BMDMs and microglia. We

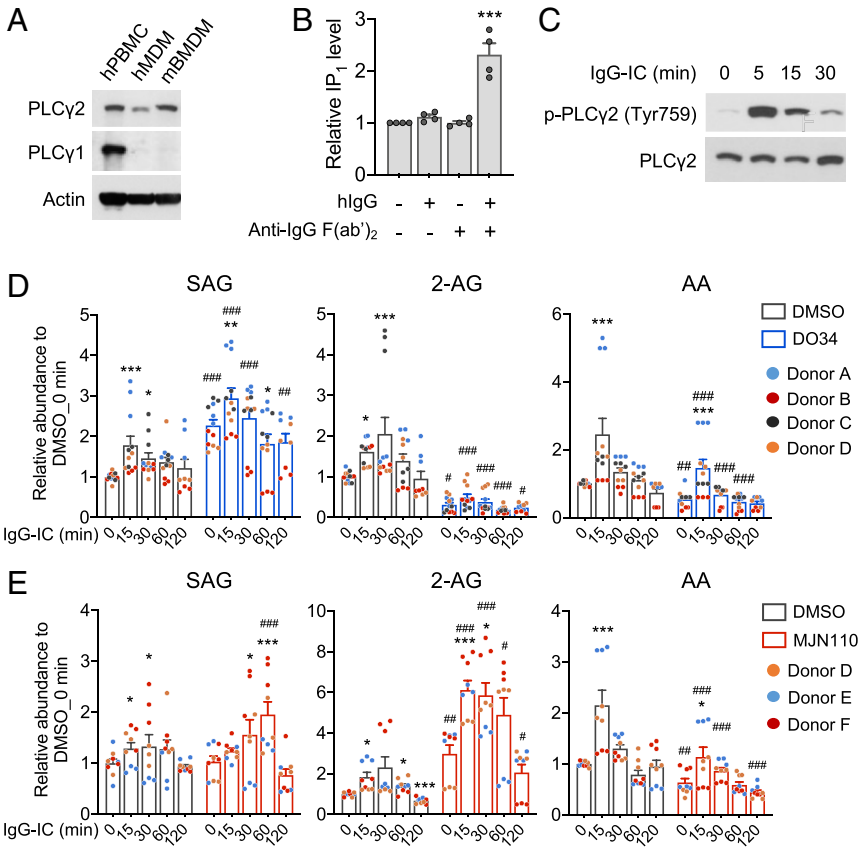

Fig. 3. FcγR cross-linking activates PLCγ2 and induces endocannabinoid production in human macrophages. (*A*) Representative immunoblots for PLCγ1 and PLCγ2 in hPBMCs, hMDMs, and mBMDMs. (*B*) IgG-IC formed by IgG and anti-IgG F(ab′)$_2$ elevated IP$_1$ content in hMDMs. hMDMs were incubated with saline or IgG (10 μg/mL, 30 min), followed by stimulation with saline or anti-IgG F(ab′)$_2$ (10 μg/mL) for 2 h prior to IP-one assay. Data represent mean values ± SEM normalized to saline-treated control group for experiments from four independent donors (four to six experimental replicates per donor). (*C*) Representative immunoblot showing IgG-IC induced a temporally restricted increase in phospho-PLCγ2 (Tyr759). hMDMs were stimulated with IgG-IC as in *B* for 0, 5, 15, and 30 min. (*D* and *E*) Effects of DO34 (*D*) and MJN110 (*E*) on FcγR cross-linking–mediated temporally restricted increases in SAG, 2-AG, and AA. hMDMs were pretreated with DMSO, DO34 (100 nM), or MJN110 (100 nM) for 2.5 h, before being incubated with IgG for another 30 min and then stimulated with IgG-IC, as described in *B* for indicated times. Data represent mean values ± SEM normalized to the DMSO_0 min group for triplicate experiments from four (*D*) or three (*E*) independent donors. Statistical tests: two-way repeated measures ANOVA, Sidak's post hoc test. $^{*}P < 0.05$, $^{**}P < 0.01$, $^{***}P < 0.001$ for stimulated group vs. 0-min stimulation; and $^{\#}P < 0.05$, $^{\#\#}P < 0.01$, $^{\#\#\#}P < 0.001$, for DO34- or MJN110- vs. DMSO-treated cells under the same stimulation condition.

confirmed expression of PLCγ2 in *Plcg2*$^{+/+}$ mBMDMs and microglia and complete loss of the protein in *Plcg2*$^{-/-}$ cells (*SI Appendix*, Fig. S5*A*). Using ABPP, we also verified expression of DAGLB in mBMDMs and microglia, whereas MGLL was only detected in microglia, but not mBMDMs (*SI Appendix*, Fig. S5 *B–D*). DAGLA was not observed in either mBMDMs or microglia. We confirmed inhibition of DAGLB in mBMDMs and microglia by DO34, which generally exhibited a similar selectivity profile in these cells to that observed in hMDMs (*SI Appendix*, Fig. S5 *C* and *D*). And also consistent with what was observed in hMDMs, MJN110 selectively inhibited MGLL and ABHD6 in microglia, with only ABHD6 being inhibited in mBMDMs due to negligible MGLL activity in these cells (*SI Appendix*, Fig. S5 *C* and *D*).

As observed in hMDMs, IgG-IC treatment increased phosphorylated PLCγ2 (p-PLCγ2) at Tyr759 in both mBMDMs and microglia, peaking as early as 5 min and sustaining at a higher level than that in untreated cells until at least 60 min (Fig. 4*A*). FcγR cross-linking also caused a significant increase in IP$_1$, which was only observed in *Plcg2*$^{+/+}$ but not *Plcg2*$^{-/-}$ mBMDMs and microglia (Fig. 4*B*). Since *Plcg2*$^{+/+}$ and *Plcg2*$^{-/-}$ mBMDMs and microglia displayed similar expression levels of FcγRI (CD64) and FcγRIII/II (CD16/32) (*SI Appendix*, Fig. S6 *A* and *B*), we interpret the loss of IgG-IC–mediated IP$_1$ production in these cells to indicate that PLCγ2 functions as the primary PLC isozyme mediating signal transduction downstream of FcγR activation.

We next assessed the DAG-2-AG-AA lipid flux in *Plcg2*$^{-/-}$ cells upon FcγR cross-linking. Similar to what was observed in hMDMs, IgG-IC treatment led to temporally restricted elevations in SAG and 2-AG in *Plcg2*$^{+/+}$ mBMDMs and microglia (Fig. 4 *C* and *D*, *SI Appendix*, Fig. S6 *C* and *D*, and Dataset S1). Unlike in hMDMs, however, IgG-IC treatment did not increase the AA content of *Plcg2*$^{+/+}$ mBMDMs and microglia (*SI Appendix*, Fig. S6 *C* and *D*). The time course for SAG and 2-AG changes differed between the two innate immune cell types, with the rate of increase and resolution being faster in mBMDMs (15 to 30 min) than microglia (45 to 180 min). In contrast, SAG and 2-AG were not increased in IgG-IC–treated *Plcg2*$^{-/-}$ mBMDMs and microglia and, in the former cells, instead a paradoxical decrease in SAG and 2-AG was observed (Fig. 4 *C* and *D* and *SI Appendix*, Fig. S6 *C* and *D*). We are unsure of the basis for this decrease, but it could suggest adaptations in DAG metabolism in the absence of PLCγ2 in mBMDMs.

We found that mBMDMs and microglia responded differently to DAGL and MGLL inhibitors. DAGL blockade substantially increased basal SAG and lowered basal 2-AG in *Plcg2*$^{+/+}$

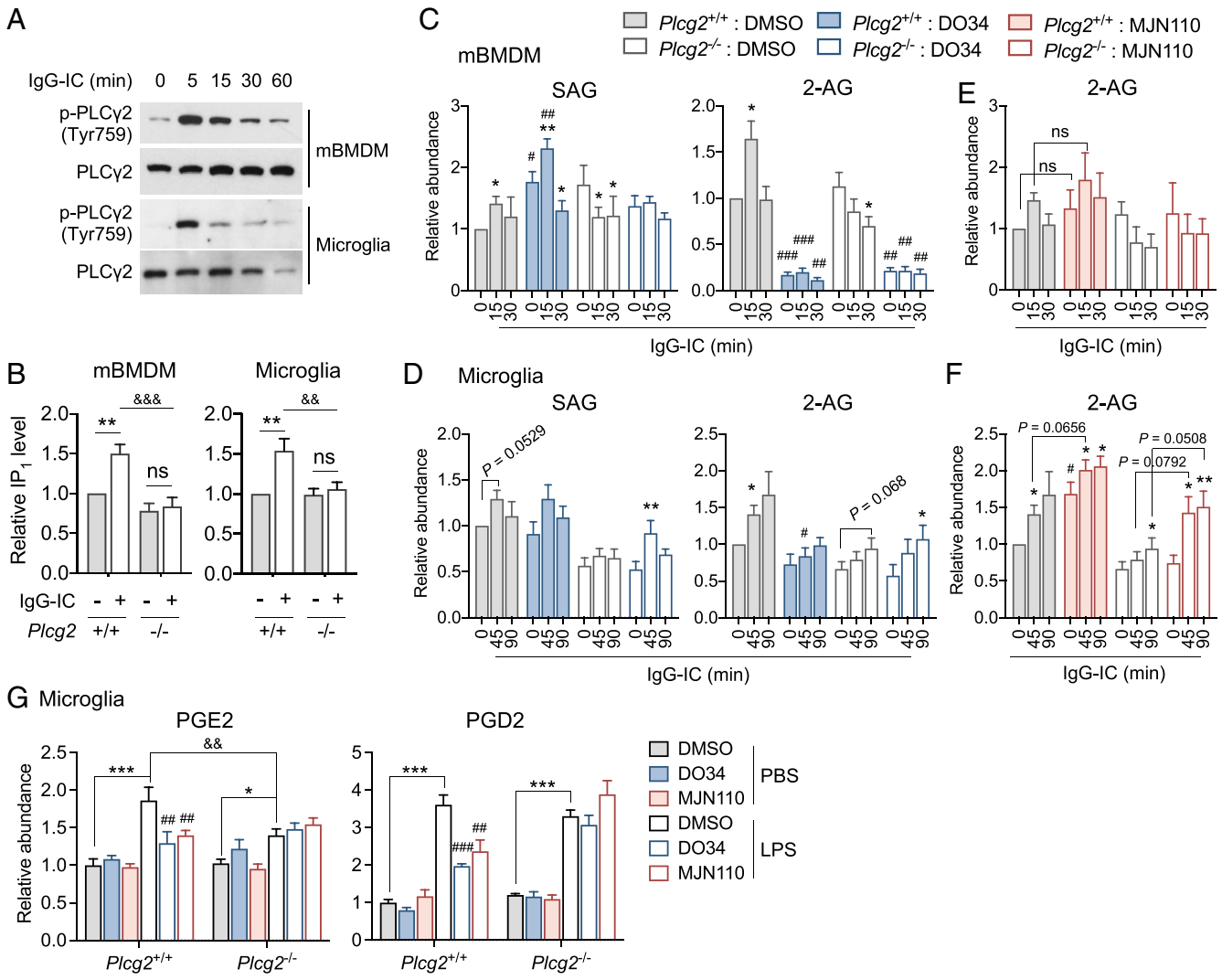

Fig. 4. PLCγ2-mediated endocannabinoid/eicosanoid production in mBMDMs and microglia. (*A*) IgG-IC induced a temporally restricted increase in phospho-PLCγ2 (Tyr759) in both mBMDMs and microglia. Cells were stimulated with IgG-IC [IgG, 20 μg/mL and anti-IgG F(ab′)$_2$, 20 and 10 μg/mL for mBMDMs and microglia, respectively] for 0 to 60 min, as indicated. (*B*) IgG-IC elevated IP_1 content in *Plcg2*$^{+/+}$, but not *Plcg2*$^{-/-}$ mBMDMs and microglia. Cells were stimulated with IgG-IC as in *A* for 2 h prior to IP_1 measurement. Data represent mean values ± SEM normalized to untreated control cells from five (mBMDMs) or eight (microglia) biologically independent experiments. Statistical tests: two-way ANOVA, Tukey's post hoc test. $^{*}P < 0.05$, $^{**}P < 0.01$ for with vs. without IgG-IC stimulation; $^{\&\&}P < 0.01$, $^{\&\&\&}P < 0.001$ for *Plcg2*$^{-/-}$ vs. corresponding *Plcg2*$^{+/+}$ group. ns, not significant. (*C–F*) Effects of DO34 and MJN110 on FcγR cross-linking–mediated temporally restricted changes in SAG and 2-AG in *Plcg2*$^{+/+}$ and *Plcg2*$^{-/-}$ mBMDMs (*C* and *E*) and microglia (*D* and *F*). Cells were pretreated with either inhibitor (100 nM) for 3 h before being stimulated with IgG-IC as indicated. For *C–F*, data represent mean values ± SEM normalized to *Plcg2*$^{+/+}$ cells at 0 min of IgG-IC stimulation from seven (mBMDMs) or six (microglia) biologically independent experiments. The SAG and 2-AG data shown in *SI Appendix*, Fig. S6 *C* and *D* were replotted as the DMSO groups in *C* and *D* and *F*, respectively, for the relevant comparisons. Statistical tests for (*C–F*): two-way repeated measures ANOVA, Sidak's post hoc test. $^{*}P < 0.05$, $^{**}P < 0.01$ for stimulated group vs. 0-min stimulation; $^{\#}P < 0.05$, $^{\#\#}P < 0.01$, $^{\#\#\#}P < 0.001$, for DO34- or MJN110- vs. DMSO-treated cells under the same stimulation condition. (*G*) Effects of DO34 and MJN110 on PGE2 and PGD2 content in *Plcg2*$^{+/+}$ and *Plcg2*$^{-/-}$ microglia following LPS treatment. Cells were pretreated with DO34 (100 nM) or MJN110 (100 nM) for 3 h before being stimulated with LPS (100 ng/mL) for another 4 h. Data represent mean values ± SEM normalized to *Plcg2*$^{+/+}$ cells treated with DMSO followed by PBS from six biologically independent experiments. Statistical tests: two-way ANOVA, Tukey's post hoc test., $^{*}P < 0.05$, $^{***}P < 0.001$ for LPS vs. the corresponding PBS stimulated group; $^{\#\#}P < 0.01$, $^{\#\#\#}P < 0.001$, for DO34- or MJN110- vs. DMSO-treated cells under the same stimulation condition; $^{\&\&}P < 0.01$ for *Plcg2*$^{-/-}$ vs. corresponding *Plcg2*$^{+/+}$ group.

mBMDMs, while also producing a striking amplification of SAG elevation in response to FcγR cross-linking in these cells (Fig. 4*C*). The latter effect was completely absent in *Plcg2*$^{-/-}$ mBMDMs (Fig. 4*C*), and DAGL inhibition also did not alter basal SAG in these cells, but still decreased their 2-AG content (Fig. 4*C*). In microglia, DAGL inhibition produced a more modest effect on basal and IgG-IC–stimulated SAG and 2-AG regardless of *Plcg2* genotype, consisting mainly of a dampening of IgG-IC–induced 2-AG in *Plcg2*$^{+/+}$ cells (Fig. 4*D*). As anticipated based on the absence of MGLL in mBMDMs, MJN110 did not alter the 2-AG content of these cells regardless of genotype or IgG-IC stimulation (Fig. 4*E*). Considering that the concentration of MJN110 used in this study also inhibited ABHD6 (*SI Appendix*, Fig. S5*C*), we conclude that this enzyme did not contribute to 2-AG metabolism in mBMDMs. In contrast, MJN110 elevated both basal and IgG-IC–stimulated 2-AG in *Plcg2*$^{+/+}$ microglia, but only increased 2-AG following IgG-IC treatment in *Plcg2*$^{-/-}$ cells (Fig. 4*F*).

Finally, we examined whether the PLCγ2-DAGL-MGLL pathway provides a source of AA for prostaglandin production in response to innate immune signals. Previously, DAGLB or MGLL

blockade has been shown to suppress LPS-induced prostaglandin production in mouse microglia (40). Consistent with this past work, we found that DO34 and MJN110 suppressed LPS-stimulated PGE2/PGD2 in *Plcg2*$^{+/+}$ microglia (LPS, 100 ng/mL, 4 h); however, neither of the compounds impacted PGE2/PGD2 in *Plcg2*$^{-/-}$ microglia, despite these cells still displaying LPS-stimulated increases in PGD2 (Fig. 4*G*). We also observed a similar lipid network in hMDMs, where LPS promoted prostaglandin production in a DAGL and MGLL inhibitor-sensitive manner (*SI Appendix*, Fig. S7).

Taken together, the aforementioned lipid profiles support the existence of a PLCγ2-DAGL-MGLL pathway that regulates both basal and stimulated DAG-2-AG flux in mouse primary innate immune cells in a manner that shares many, but not all features in common with hMDMs. One notable difference was the robust expression of MGLL in hMDMs, but not mBMDMs. Some of the unexpected properties of *Plcg2*$^{-/-}$ microglia, such as the apparent loss of regulation of both basal 2-AG and LPS-stimulated prostaglandins by DAGL/MGLL, further pointed to the potential for adapative changes caused by genetic disruption of PLCγ2.

PLCγ2 Loss Causes Major Transcriptomic and Proteomic Changes in Microglia. We were interested in further understanding the apparent lipid pathway adaptations and broader biochemical state of *Plcg2*$^{-/-}$ microglia, and therefore compared their transcriptional and proteomic profiles to those of *Plcg2*$^{+/+}$ microglia by RNA sequencing (RNA-seq) and MS-based quantitative proteomics, respectively. RNA-seq revealed substantial transcriptional changes in *Plcg2*$^{-/-}$ microglia totaling 1,811 differentially expressed genes (fold-change > 1.5, adjusted P value < 0.01; 11.3% of all quantified transcripts), including 892 up-regulated and 919 down-regulated in comparison to *Plcg2*$^{+/+}$ microglia cells (Fig. 5*A* and Dataset S2). We noted that several gene-expression markers of disease-associated microglia (*Trem2*, *Lpl*, *Itgax*, *Spp1*, *Cd9*, *Csf1*, *Cd63*), lysosomal function (*Gusb*, *Ctsl*, *Ctsd*, *Ctsk*), phagocytosis of apoptotic cells (*Cd36*, *Mfge8*), and extracellular matrix degradation (*Mmp12*, *Mmp13*, *Mmp19*) were reduced in *Plcg2*$^{-/-}$ compared with *Plcg2*$^{+/+}$ microglia (Fig. 5*A*). On the other hand, genes involved in innate immune responses, including those encoding complement components (*C1qa*, *C1qb*), MHC class I (*H2-Q4*, *H2-Q5*) and class II components (*H2-Aa*, *H2-Ab1*, *H2-Eb1*, *Cd74*), inflammatory chemokines (*Ccl2*, *Ccl5*, *Ccl7*, *Ccl8*, *Ccl12*, *Cxcl9*, *Cxcl10*), and genes that are part of the interferon response (*Ifit1*, *Ifit2*, *Ifit3*, *Isg15*, *Stat1*, *Stat2*, *Ifitm3*), were elevated in *Plcg2*$^{-/-}$ microglia. Additionally, the Ms4a transmembrane family genes, such as *Ms4a4a* and *Ms4a4b*, genetic variants of which have been linked to AD risk (50, 51) and have been shown to modulate soluble TREM2 in cerebrospinal fluid (52), were also substantially increased in *Plcg2*$^{-/-}$ microglia (Fig. 5*A*).

Specific enzymes involved in C20:4 lipid metabolism were also altered in *Plcg2*$^{-/-}$ microglia, including not only *Daglb* (~2-fold reduction), but also *Dgke* (~2-fold reduction), and *Mboat7* (~1.5-fold increase) (Fig. 5*B*). Parallel quantitative proteomic analysis of the *Plcg2*$^{+/+}$ and *Plcg2*$^{-/-}$ microglia revealed a good overall correlation with the transcriptional profile (Pearson's correlation $r = 0.57$, $P < 0.0001$) (Fig. 5*C*) and provided additional evidence for bidirectional changes in the AA-liberating enzymes DAGLB and PLA2G4A (Fig. 5*B*). These data, when combined with our lipid-profiling results, provide a potential model to explain the different responses of *Plcg2*$^{+/+}$ and *Plcg2*$^{-/-}$ microglia to DAGL and MGLL inhibitors (Fig. 5*D*). In this model, the concomitant reductions in DAGLB and elevations in PLA2G4A in *Plcg2*$^{-/-}$ microglia may shift the relative pathway contributions to LPS-induced PGE2/PGD2 production, such that PLA2G4A becomes the primary node of control, rendering the prostaglandin content of *Plcg2*$^{-/-}$ microglia insensitive to DAGL and MGLL inhibitors.

***Plcg2*$^{-/-}$ Mice Display Defects in LPS-Induced Brain Prostaglandins and Microglial Activation.** We were finally curious to understand how the spectrum of biochemical changes observed in *Plcg2*$^{-/-}$ microglia might affect lipid metabolism and microglia function in vivo. Toward this end, we exposed *Plcg2*$^{+/+}$ and *Plcg2*$^{-/-}$ mice to a peripheral LPS challenge, which has been shown to cause central inflammation accompanied by an increase in microglia activation reflected in proinflammatory cytokine expression that peaks at 2 to 4 h and morphological changes accompanied by expression of the activation marker CD68 being evident at 24 to 48 h (53–56). We accordingly treated *Plcg2*$^{+/+}$ and *Plcg2*$^{-/-}$ mice with low-dose LPS intraperitoneally (1 mg/kg, single dose) for 4 or 48 h and analyzed their brain lipid profiles at both time points, while focusing measurement of cytokines and microglia activation state at 4 and 48 h, respectively (*SI Appendix*, Fig. S8*A*).

We found that PGE2, but not other measured lipids (e.g., SAG, 2-AG, AA), was elevated in brain tissue from *Plcg2*$^{+/+}$ mice at both 4 and 48 h post-LPS treatment (Fig. 6 *A* and *B*, *SI Appendix*, Fig. S8 *B* and *C*, and Dataset S1). Brain PGD2 was also elevated at 4 h, but not 48 h in these animals. In contrast, *Plcg2*$^{-/-}$ mice showed impaired induction of PGE2 and PGD2 by LPS compared to *Plcg2*$^{+/+}$ littermates, and this effect was most pronounced at 48 h, where the brain PGE2 content did not differ between vehicle- and LPS-treated *Plcg2*$^{-/-}$ mice (Fig. 6*B*). In line with previous studies (56), we observed a marked increase in brain proinflammatory cytokines and chemokines, including interleukin (IL)-6, tumor necrosis factor (TNF)-α, IL-1β, and CXCL1, at 4 h post-LPS treatment in *Plcg2*$^{+/+}$ mice (*SI Appendix*, Fig. S8*D*). A generally similar response was observed in *Plcg2*$^{-/-}$ mice, suggesting a limited role for PLCγ2 in early inflammatory responses to LPS challenge. At 48 h post-LPS treatment, and consistent with previous reports (53, 55), flow cytometry analysis of CD11b^{+}/CD45^{int} brain cells (*SI Appendix*, Fig. S8*E*) confirmed heightened signals for several markers of microglial activation in *Plcg2*$^{-/-}$ mice, including CD11b, CD45, and CD68 (Fig. 6*C*), as well as forward scatter (correlating with cell size) and side scatter (correlating with cell granularity) signals (*SI Appendix*, Fig. S8*F*). Most of these microglial markers were similarly increased in LPS-treated *Plcg2*$^{-/-}$ mice, with the exception of the prophagocytic marker CD68, which was markedly suppressed in these animals (Fig. 6*C*). The total percentage of brain microglia was also slightly reduced in *Plcg2*$^{-/-}$ mice (26.6% vs. 32.0% of total brain live cells, $P = 0.0084$), but this feature was unaffected by LPS treatment (Fig. 6*D*).

Taken together, these results suggest that loss of PLCG2 has a discrete, rather than generalized impact on mouse microglia function in vivo that is reflected in impaired prostaglandin production and possibly CD68-related functions (e.g., phagocytosis) in response to inflammatory stimuli. We interpret the reduction in brain prostaglandin content to reflect the specialized role that microglia play in regulating this bioactive lipid class in the nervous system. This conclusion is also supported by studies of other enzymes in the PLCγ2-DAGL-MGLL pathway (40, 57), such as DAGLB, which, like PLCγ2, is preferentially expressed in microglia compared to other brain cell types (*SI Appendix*, Fig. S8*G*) (https://www.brainrnaseq.org/) (58) and, when disrupted, suppresses brain prostaglandins while sparing bulk 2-AG content (40). We accordingly believe that our studies, when integrated with past work, establish the PLCγ2-DAGLB-MGLL pathway as an important regulator of endocannabinoid–eicosanoid cross-talk and microglia activation in vivo.

Discussion

Recent monogenic and genome-wide association discoveries have illuminated functional connections between enzymes involved in bioactive lipid metabolism and immunological and neurological disorders, including autoimmunity (21, 22) and neurodegeneration (2, 5, 10, 29). In many cases, however, our understanding of the lipid networks regulated by these enzymes

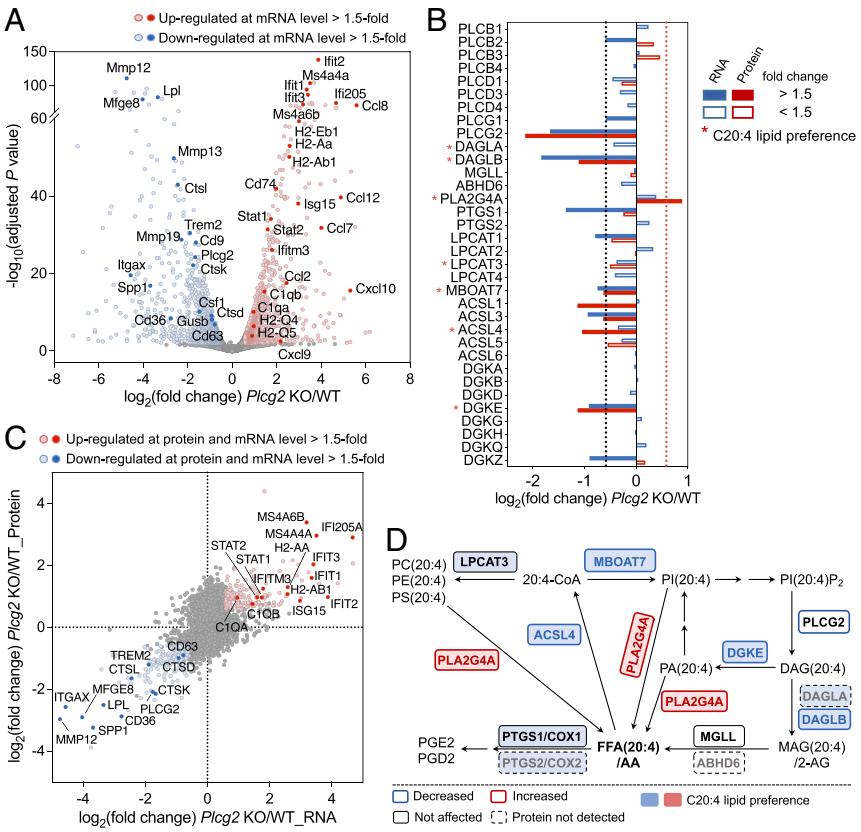

Fig. 5. PLCγ2 deficiency causes substantial transcriptomic and proteomic changes in microglia. (*A*) Volcano plot showing differentially expressed genes expressed in *Plcg2*$^{+/+}$ and *Plcg2*$^{-/-}$ microglia as determined by RNA-seq. Data represent mean values from three biologically independent experiments. (*B*) Differential expression of C20:4 lipid metabolism enzymes and the corresponding closely related isozymes at mRNA and protein level in *Plcg2*$^{-/-}$ vs. *Plcg2*$^{+/+}$ microglia. The dashed lines represent fold-change > 1.5. (*C*) Correlation analysis of transcriptomic and proteomic data from *Plcg2*$^{+/+}$ and *Plcg2*$^{-/-}$ microglia. For *B* and *C*, quantitative proteomic data represent mean values from five biologically independent experiments. (*D*) Model for rewiring of C20:4 lipid metabolic network following PLCγ2 loss in microglia. Enzymes shown as increased or decreased are those with fold-change > 1.5 at protein level. For all panels, a cutoff of adjusted $P < 0.01$ (two-sided Student's *t* test, Benjamini–Hochberg false-discovery rate) was set for genes or proteins up-regulated or down-regulated > 1.5-fold.

remains incomplete. The immune cell-restricted phospholipase PLCγ2, mutations in which have been linked to human immunological (21–24) and neurological disorders (10, 29), as well as cancer drug resistance (26–28, 36), hydrolyzes PIP_2 at the plasma membrane to generate two second messengers, IP_3 and DAG. While it is generally acknowledged that IP_3 triggers cellular Ca^{2+} signaling (59) and that DAG activates effector proteins, such as protein kinase C (60), the additional role of PLC-generated DAG as a precursor for bioactive lipids, such as endocannabinoids and eicosanoids, remains understudied, in particular in immune cells. Here, we have uncovered that the activation of PLCγ2, through disease-relevant mutations or FcR signaling, stimulates the production of DAG, 2-AG, and prostaglandins in primary human and mouse immune cells through a pathway that involves DAGL and MGLL enzymes.

By studying PLCγ2-regulated lipid networks in three myeloid cell types—hMDMs, mBMDMs, and mouse microglia—we gained knowledge of the shared and differential composition of these networks across the cell types, as well as their responsivity to distinct stimuli (e.g., FcγR activation, LPS). For example, we found that hMDMs strongly express MGLL (*SI Appendix*, Fig. S3*A*), while this enzyme is absent from mBMDMs (*SI Appendix*, Fig. S5 *B* and *C*). While we do not fully understand the functional implications of this difference, it likely contributes to the greater apparent flux leading to 2-AG and AA production following FcγR activation in hMDMs compared to mBMDMs. And, from a tactical perspective, the findings underscore the importance of studying primary human immune cells when assessing bioactive lipid networks, as their composition may differ between human and mouse cells. Additionally, we found that basal and stimulated SAG content was substantially elevated in mBMDMs by DAGL inhibition (Fig. 4*C*), while being unaffected in microglia (Fig. 4*D*), even though reductions in 2-AG were observed in both cell types. These observations suggest that SAG pools may be differentially regulated by DAGL and possibly other enzymes that utilize SAG as substrate (e.g., DAG kinases) in each innate immune cell type. We also found that IgG-IC and LPS treatment led to differential coupling of the PLCγ2-DAGL-MGLL pathway to downstream prostaglandin production, as only LPS treatment was found to increase PGE2/PGD2 and this change was sensitive to DAGL and MGLL inhibition. These results may indicate that the induction of PTGS2 (COX-2) following LPS treatment is required to connect the PLCγ2-DAGL-MGLL pathway to prostaglandin production.

Genetic or pharmacologic inactivation of DAGLB and MGLL has been shown to impair LPS-induced endocannabinoid-prostaglandin cross-talk in mouse microglia (40). Here we found that, in the absence of PLCγ2, DAGL and MGLL inhibitors no longer suppress LPS-induced prostaglandin production in microglia (Fig. 4*G*). These observations support that, in WT microglia, PLCγ2, DAGLB, and MGLL function together in a DAG-2-AG-AA pathway to regulate LPS-induced prostaglandin production.

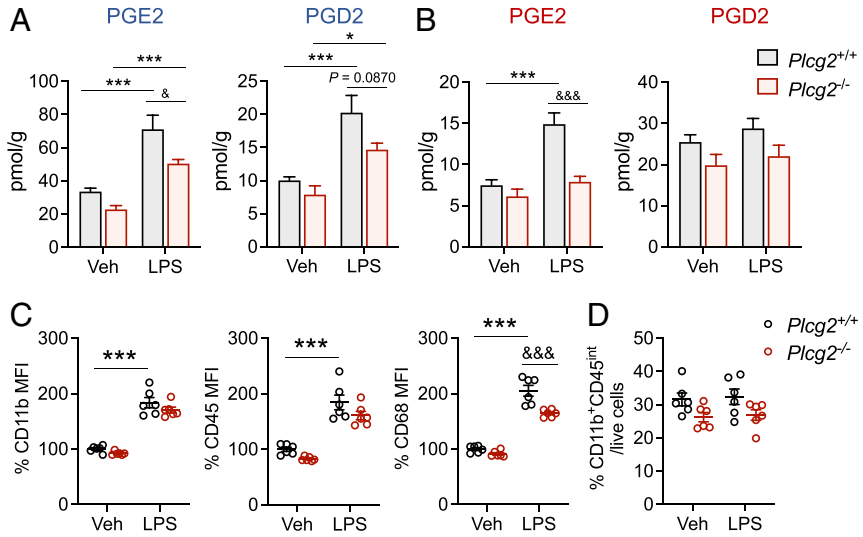

Fig. 6. Genetic disruption of PLCγ2 impairs LPS-induced prostaglandin production and specific features of microglia activation in vivo. (*A* and *B*) PGE2 and PGD2 content of brain tissue from *Plcg2*$^{+/+}$ and *Plcg2*$^{-/-}$ mice basally or following LPS treatment for 4 h (*A*) or 48 h (*B*). (*C* and *D*) Relative fluorescent signals for CD11b, CD45, and CD68 in microglia cells (identified as CD11b^{+}CD45^{int}) (*C*) and percentage of microglia cell population in total live cells (*D*) from brain tissue of *Plcg2*$^{+/+}$ and *Plcg2*$^{-/-}$ mice following vehicle or LPS treatment for 48 h. Corrected mean fluorescent intensity (MFI) for each marker was normalized to the average of the *Plcg2*$^{+/+}$ vehicle control group. All data represent mean values ± SEM for six biologically independent experiments. Statistical significance was calculated with two-way ANOVA, Tukey's post hoc test. $^{*}P < 0.05$, $^{***}P < 0.001$ for LPS vs. Veh-treated mice; $^{\&}P < 0.05$, $^{\&\&\&}P < 0.001$ for *Plcg2*$^{-/-}$ vs. corresponding *Plcg2*$^{+/+}$ group.

Interpreting the output of this pathway following PLCγ2 disruption is more complicated due to the widespread transcriptomic and proteomic changes observed in *Plcg2*$^{-/-}$ microglia (Fig. 5 *A* and *C*), including not only reductions in additional pathway components (DAGLB), but also elevations in other enzymes that furnish AA for prostaglandin production (PLA2G4A) (39) (Fig. 5*B*). These adaptations may explain why LPS still promotes prostaglandin production in *Plcg2*$^{-/-}$ microglia, but in a manner that is independent of DAGL and MGLL (Fig. 4*G*). We note, however, that LPS-induced prostaglandin production was impaired in the CNS of *Plcg2*$^{-/-}$ mice (Fig. 6 *A* and *B*), suggesting that cultured microglia may not fully recapitulate the physiological consequences of PLCγ2 loss to bioactive lipid production in vivo.

When attempting to assess the functional contributions of PLCγ2 to neuroimmunology in vivo, we were surprised to find that *Plcg2*$^{-/-}$ mice maintained WT cytokine and chemokine responses to LPS treatment in the CNS (*SI Appendix*, Fig. S8*D*). Additionally, several biomarkers of microglia activation were also similar between LPS-treated *Plcg2*$^{+/+}$ and *Plcg2*$^{-/-}$ mice. One notable exception was a reduction in CD68 positivity for microglia from LPS-treated *Plcg2*$^{-/-}$ mice. While the changes in microglial function imparted by CD68 expression are still incompletely understood, this protein is generally considered a marker of greater phagocytic activity (61–63), and recent studies of PLCG2-disrupted human iPSC-derived microglia also revealed impaired phagocytosis (30). How the impact of PLCγ2 loss on CD68^{+} microglia, combined with the suppression of prostaglandins, may impact broader neuroimmunobiological responses to innate stimuli like LPS, is an important topic for future investigation. Also, while we assume that PLCγ2 regulation of stimulated prostaglandin production in vivo reflects the action of the DAG-2-AG-AA pathway involving DAGL and MGLL enzymes, as studied herein, we do not know the extent to which this pathway versus IP_3 signaling mediates the suppression of CD68 positivity observed in LPS-treated *Plcg2*$^{-/-}$ mice. We further call attention to the possibility that PLCs may utilize other lipid substrates beyond PIP_2 [e.g., phosphatidylinositol 4-phosphate (64)], which would uncouple downstream DAG-2-AG-AA lipid effects from IP_3 signaling. We can nonetheless conclude from our studies that PLCγ2 likely functions in a microglia-restricted manner, as bulk 2-AG content in the brain was unaffected in *Plcg2*$^{-/-}$ mice (*SI Appendix*, Fig. S8 *B* and *C*). This finding, which is consistent with the expression of PLCγ2 primarily in microglia among brain cell types (20, 65–67), further suggests that microglia serve as the main source for PGE2 production in the CNS following LPS treatment, which may also involve the concerted action of mPGES-1 and COX-2 (68).

From a translational perspective, it is encouraging that PLCγ2 disruption appears to modulate microglial function without exerting broader effects on endocannabinoid signaling in the brain, which likely reflects the contributions of other PLC isozymes in brain cell types, such as astrocytes and neurons (58, 69, 70). These data suggest that inhibitors or activators of PLCγ2 may be expected to influence principally immunological processes in the CNS. Also supporting this conclusion, PLCγ2 has recently been shown to signal downstream of TREM2 in microglia to mediate survival, phagocytosis, and lipid metabolism (30). Given that TREM2 loss also attenuates microglia activation, as indicated particularly by reduced CD68 expression in animal models of neurological disease (71–73), our observations add to an emerging model where TREM2 and PLCγ2 form a signal transduction pathway important for modulating specific functional properties of microglia. The extent to which this pathway can be safely stimulated by pharmacological agents is an important future consideration. The LOAD-protective rare PLCγ2_P522R variant was recently shown to act as a weakly functional hypermorph (20) and to promote protective microglial function associated with TREM2 signaling in vitro and in mice (30, 34, 74), and our data also support the conclusion that PLCγ2_P522R shows much more tempered activity compared to other autoimmune and cancer therapy-related mutants of this enzyme (e.g., S707Y, L845F). Pharmacological tools for promoting PLCγ2 activation may need to mimic this gentle stimulatory outcome to maximize productive versus deleterious activation of innate immune signaling.

We finally conclude by emphasizing the need for selective chemical probes that not only activate, but also inhibit PLCγ2. Our findings in *Plcg2*$^{-/-}$ microglia underscore the potential for

substantial proteomic adaptations caused by chronic loss of PLCγ2. The discovery of inhibitors would enable investigations of PLCγ2 function in acute, graded, and reversible paradigms while avoiding potential compensatory changes caused by complete, sustained loss of this enzyme. We also speculate that the coupling of PLCγ2 to endocannabinoid and eicosanoid pathways discovered herein may point to DAGL and MGLL inhibitors as a way to modulate immune pathologies driven by the activation of PLCγ2.

Materials and Methods

An extended section with detailed information on materials, reagents, and procedures is provided in *SI Appendix, Supporting Experimental Procedures*. All studies using blood from human volunteers follow protocols approved by The Scripps Research Institute (TSRI) Institutional Review Board (protocol #IRB-15-6682). Written informed consent was obtained from each healthy donor following completion of an application to the donor program, screening and acceptance for enrollment into the TSRI Normal Blood Donor Services. Each donor is then provided with a Blood Donor Information Form, which describes the research project and ensures all donations are de-identified. Animal experiments were carried out in compliance with TSRI institutional animal protocols (Institutional Animal Care and Use Committee #09-0041).

Generation of Primary Macrophages and Microglia. PBMCs were purified and hMDMs were generated following a previously described method (75). Mouse BMDMs and neonatal microglia were generated as described previously (40, 76) and in *SI Appendix, Supporting Experimental Procedures*.

Biochemical Studies. Lipid extraction and analysis for cell and brain samples, MS-based ABPP analysis, and proteomic characterization of *Plcg2*$^{+/+}$ and *Plcg2*$^{-/-}$ microglia were performed as described previously (40, 77, 78) and in *SI Appendix, Supporting Experimental Procedures*.

Data Availability. Next-generation sequencing data have been deposited in the National Center for Biotechnology Information Gene Expression Omnibus (accession no. GSE180274) (79). The mass spectrometry proteomics data have been deposited to the ProteomeXchange Consortium (80) via the PRoteomics IDEntifications Database (PRIDE) partner repository (dataset identifier PXD027350) (81). All other study data are included in the main text and supporting information.

ACKNOWLEDGMENTS. This work was supported by the NIH Grant (DA037660) and the Life Sciences Research Foundation Postdoctoral Fellowship (to H.J.).

1. H. Koss, T. D. Bunney, S. Behjati, M. Katan, Dysfunction of phospholipase Cγ in immune disorders and cancer. *Trends Biochem. Sci.* **39**, 603–611 (2014).
2. A. Johansen *et al.*, Mutations in MBOAT7, encoding lysophosphatidylinositol acyltransferase I, lead to intellectual disability accompanied by epilepsy and autistic features. *Am. J. Hum. Genet.* **99**, 912–916 (2016).
3. C. Tesson *et al.*, Alteration of fatty-acid-metabolizing enzymes affects mitochondrial form and function in hereditary spastic paraplegia. *Am. J. Hum. Genet.* **91**, 1051–1064 (2012).
4. J. H. Schuurs-Hoeijmakers *et al.*; FORGE Canada Consortium, Mutations in DDHD2, encoding an intracellular phospholipase A(1), cause a recessive form of complex hereditary spastic paraplegia. *Am. J. Hum. Genet.* **91**, 1073–1081 (2012).
5. T. Fiskerstrand *et al.*, Mutations in ABHD12 cause the neurodegenerative disease PHARC: An inborn error of endocannabinoid metabolism. *Am. J. Hum. Genet.* **87**, 410–417 (2010).
6. A. Guemez-Gamboa *et al.*, Inactivating mutations in MFSD2A, required for omega-3 fatty acid transport in brain, cause a lethal microcephaly syndrome. *Nat. Genet.* **47**, 809–813 (2015).
7. T. Aikawa, M. L. Holm, T. Kanekiyo, ABCA7 and pathogenic pathways of Alzheimer's disease. *Brain Sci.* **8**, 27 (2018).
8. F. Liao, H. Yoon, J. Kim, Apolipoprotein E metabolism and functions in brain and its role in Alzheimer's disease. *Curr. Opin. Lipidol.* **28**, 60–67 (2017).
9. J. L. Goldstein, M. S. Brown, A century of cholesterol and coronaries: From plaques to genes to statins. *Cell* **161**, 161–172 (2015).
10. R. Sims *et al.*; ARUK Consortium; GERAD/PERADES, CHARGE, ADGC, EADI, Rare coding variants in PLCG2, ABI3, and TREM2 implicate microglial-mediated innate immunity in Alzheimer's disease. *Nat. Genet.* **49**, 1373–1384 (2017).
11. L. Cristino, T. Bisogno, V. Di Marzo, Cannabinoids and the expanded endocannabinoid system in neurological disorders. *Nat. Rev. Neurol.* **16**, 9–29 (2020).
12. H. Harizi, J. B. Corcuff, N. Gualde, Arachidonic-acid-derived eicosanoids: Roles in biology and immunopathology. *Trends Mol. Med.* **14**, 461–469 (2008).
13. E. A. Dennis, P. C. Norris, Eicosanoid storm in infection and inflammation. *Nat. Rev. Immunol.* **15**, 511–523 (2015).
14. C. T. Robb, M. Goepp, A. G. Rossi, C. Yao, Non-steroidal anti-inflammatory drugs, prostaglandins, and COVID-19. *Br. J. Pharmacol.* **177**, 4899–4920 (2020).
15. G. Donvito *et al.*, The endogenous cannabinoid system: A budding source of targets for treating inflammatory and neuropathic pain. *Neuropsychopharmacology* **43**, 52–79 (2018).
16. L. Cocco, M. Y. Follo, L. Manzoli, P. G. Suh, Phosphoinositide-specific phospholipase C in health and disease. *J. Lipid Res.* **56**, 1853–1860 (2015).
17. L. Zhu, C. Jones, G. Zhang, The role of phospholipase C signaling in macrophage-mediated inflammatory response. *J. Immunol. Res.* **2018**, 5201759 (2018).
18. M. Katan, S. Cockcroft, Phospholipase C families: Common themes and versatility in physiology and pathology. *Prog. Lipid Res.* **80**, 101065 (2020).
19. R. Wen, S. T. Jou, Y. Chen, A. Hoffmeyer, D. Wang, Phospholipase C gamma 2 is essential for specific functions of Fc epsilon R and Fc gamma R. *J. Immunol.* **169**, 6743–6752 (2002).
20. L. Magno *et al.*, Alzheimer's disease phospholipase C-gamma-2 (PLCG2) protective variant is a functional hypermorph. *Alzheimers Res. Ther.* **11**, 16 (2019).
21. M. J. Ombrello *et al.*, Cold urticaria, immunodeficiency, and autoimmunity related to PLCG2 deletions. *N. Engl. J. Med.* **366**, 330–338 (2012).
22. Q. Zhou *et al.*, A hypermorphic missense mutation in PLCG2, encoding phospholipase Cγ2, causes a dominantly inherited autoinflammatory disease with immunodeficiency. *Am. J. Hum. Genet.* **91**, 713–720 (2012).
23. J. F. Neves *et al.*, Novel *PLCG2* mutation in a patient with APLAID and Cutis Laxa. *Front. Immunol.* **9**, 2863 (2018).
24. R. A. Gbadegesin *et al.*; Mid-West Pediatric Nephrology Consortium, HLA-DQA1 and PLCG2 are candidate risk loci for childhood-onset steroid-sensitive nephrotic syndrome. *J. Am. Soc. Nephrol.* **26**, 1701–1710 (2015).
25. Y. Kaymaz *et al.*, Comprehensive transcriptome and mutational profiling of endemic Burkitt lymphoma reveals EBV type-specific differences. *Mol. Cancer Res.* **15**, 563–576 (2017).
26. D. Jones *et al.*, PLCG2 C2 domain mutations co-occur with BTK and PLCG2 resistance mutations in chronic lymphocytic leukemia undergoing ibrutinib treatment. *Leukemia* **31**, 1645–1647 (2017).
27. J. A. Woyach *et al.*, Resistance mechanisms for the Bruton's tyrosine kinase inhibitor ibrutinib. *N. Engl. J. Med.* **370**, 2286–2294 (2014).
28. M. Y. Follo *et al.*, Response of high-risk MDS to azacitidine and lenalidomide is impacted by baseline and acquired mutations in a cluster of three inositide-specific genes. *Leukemia* **33**, 2276–2290 (2019).
29. S. J. van der Lee *et al.*; DESGESCO (Dementia Genetics Spanish Consortium), EADB (Alzheimer Disease European DNA biobank); EADB (Alzheimer Disease European DNA biobank); IFGC (International FTD-Genomics Consortium), IPDGC (The International Parkinson Disease Genomics Consortium); IPDGC (The International Parkinson Disease Genomics Consortium); RiMod-FTD (Risk and Modifying factors in Frontotemporal Dementia); Netherlands Brain Bank (NBB); GIFT (Genetic Investigation in Frontotemporal Dementia and Alzheimer's Disease) Study Group, A nonsynonymous mutation in PLCG2 reduces the risk of Alzheimer's disease, dementia with Lewy bodies and frontotemporal dementia, and increases the likelihood of longevity. *Acta Neuropathol.* **138**, 237–250 (2019).
30. B. J. Andreone *et al.*, Alzheimer's-associated PLCγ2 is a signaling node required for both TREM2 function and the inflammatory response in human microglia. *Nat. Neurosci.* **23**, 927–938 (2020).
31. Y. Wang *et al.*, TREM2 lipid sensing sustains the microglial response in an Alzheimer's disease model. *Cell* **160**, 1061–1071 (2015).
32. C. Walliser *et al.*, Functional characterization of phospholipase C-γ_2 mutant protein causing both somatic ibrutinib resistance and a germline monogenic autoinflammatory disorder. *Oncotarget* **9**, 34357–34378 (2018).
33. M. Wist *et al.*, Noncatalytic Bruton's tyrosine kinase activates PLCγ_2 variants mediating ibrutinib resistance in human chronic lymphocytic leukemia cells. *J. Biol. Chem.* **295**, 5717–5736 (2020).
34. M. Takalo *et al.*, The Alzheimer's disease-associated protective Plcγ2-P522R variant promotes immune functions. *Mol. Neurodegener.* **15**, 52 (2020).
35. C. Walliser *et al.*, The phospholipase Cγ2 mutants R665W and L845F identified in ibrutinib-resistant chronic lymphocytic leukemia patients are hypersensitive to the Rho GTPase Rac2 protein. *J. Biol. Chem.* **291**, 22136–22148 (2016).
36. I. E. Ahn *et al.*, Clonal evolution leading to ibrutinib resistance in chronic lymphocytic leukemia. *Blood* **129**, 1469–1479 (2017).
37. E. Trinquet *et al.*, D-myo-inositol 1-phosphate as a surrogate of D-myo-inositol 1,4,5-tris phosphate to monitor G protein-coupled receptor activation. *Anal. Biochem.* **358**, 126–135 (2006).
38. A. Tanimura *et al.*, The endocannabinoid 2-arachidonoylglycerol produced by diacylglycerol lipase alpha mediates retrograde suppression of synaptic transmission. *Neuron* **65**, 320–327 (2010).
39. K. L. Hsu *et al.*, DAGLβ inhibition perturbs a lipid network involved in macrophage inflammatory responses. *Nat. Chem. Biol.* **8**, 999–1007 (2012).
40. A. Viader *et al.*, A chemical proteomic atlas of brain serine hydrolases identifies cell type-specific pathways regulating neuroinflammation. *eLife* **5**, e12345 (2016).
41. T. Bisogno *et al.*, Cloning of the first sn1-DAG lipases points to the spatial and temporal regulation of endocannabinoid signaling in the brain. *J. Cell Biol.* **163**, 463–468 (2003).
42. T. P. Dinh *et al.*, Brain monoglyceride lipase participating in endocannabinoid inactivation. *Proc. Natl. Acad. Sci. U.S.A.* **99**, 10819–10824 (2002).
43. D. Ogasawara *et al.*, Rapid and profound rewiring of brain lipid signaling networks by acute diacylglycerol lipase inhibition. *Proc. Natl. Acad. Sci. U.S.A.* **113**, 26–33 (2016).
44. M. J. Niphakis *et al.*, Evaluation of NHS carbamates as a potent and selective class of endocannabinoid hydrolase inhibitors. *ACS Chem. Neurosci.* **4**, 1322–1332 (2013).

45. Y. Liu, M. P. Patricelli, B. F. Cravatt, Activity-based protein profiling: The serine hydrolases. *Proc. Natl. Acad. Sci. U.S.A.* **96**, 14694–14699 (1999).
46. N. Jessani *et al*., A streamlined platform for high-content functional proteomics of primary human specimens. *Nat. Methods* **2**, 691–697 (2005).
47. D. A. Bachovchin *et al*., Superfamily-wide portrait of serine hydrolase inhibition achieved by library-versus-library screening. *Proc. Natl. Acad. Sci. U.S.A.* **107**, 20941–20946 (2010).
48. M. Alhouayek, J. Masquelier, P. D. Cani, D. M. Lambert, G. G. Muccioli, Implication of the anti-inflammatory bioactive lipid prostaglandin D2-glycerol ester in the control of macrophage activation and inflammation by ABHD6. *Proc. Natl. Acad. Sci. U.S.A.* **110**, 17558–17563 (2013).
49. F. Ozdener, C. Dangelmaier, B. Ashby, S. P. Kunapuli, J. L. Daniel, Activation of phospholipase Cgamma2 by tyrosine phosphorylation. *Mol. Pharmacol.* **62**, 672–679 (2002).
50. J. C. Lambert *et al*.; European Alzheimer's Disease Initiative (EADI); Genetic and Environmental Risk in Alzheimer's Disease; Alzheimer's Disease Genetic Consortium; Cohorts for Heart and Aging Research in Genomic Epidemiology, Meta-analysis of 74,046 individuals identifies 11 new susceptibility loci for Alzheimer's disease. *Nat. Genet.* **45**, 1452–1458 (2013).
51. K. L. Huang *et al*.; International Genomics of Alzheimer's Project; Alzheimer's Disease Neuroimaging Initiative, A common haplotype lowers PU.1 expression in myeloid cells and delays onset of Alzheimer's disease. *Nat. Neurosci.* **20**, 1052–1061 (2017).
52. Y. Deming *et al*., The *MS4A* gene cluster is a key modulator of soluble TREM2 and Alzheimer's disease risk. *Sci. Transl. Med.* **11**, eaau2291 (2019).
53. D. Tejera *et al*., Systemic inflammation impairs microglial Aβ clearance through NLRP3 inflammasome. *EMBO J.* **38**, e101064 (2019).
54. G. Kleinberger *et al*., The FTD-like syndrome causing TREM2 T66M mutation impairs microglia function, brain perfusion, and glucose metabolism. *EMBO J.* **36**, 1837–1853 (2017).
55. A. Bhattacharya *et al*., Neuropsychopharmacology of JNJ-55308942: Evaluation of a clinical candidate targeting P2X7 ion channels in animal models of neuroinflammation and anhedonia. *Neuropsychopharmacology* **43**, 2586–2596 (2018).
56. D. M. Norden, P. J. Trojanowski, E. Villanueva, E. Navarro, J. P. Godbout, Sequential activation of microglia and astrocyte cytokine expression precedes increased Iba-1 or GFAP immunoreactivity following systemic immune challenge. *Glia* **64**, 300–316 (2016).
57. D. K. Nomura *et al*., Endocannabinoid hydrolysis generates brain prostaglandins that promote neuroinflammation. *Science* **334**, 809–813 (2011).
58. Y. Zhang *et al*., An RNA-sequencing transcriptome and splicing database of glia, neurons, and vascular cells of the cerebral cortex. *J. Neurosci.* **34**, 11929–11947 (2014).
59. M. J. Berridge, Inositol trisphosphate and calcium signalling. *Nature* **361**, 315–325 (1993).
60. K. P. Huang, The mechanism of protein kinase C activation. *Trends Neurosci.* **12**, 425–432 (1989).
61. J. A. Nicoll *et al*., Neuropathology of human Alzheimer disease after immunization with amyloid-beta peptide: A case report. *Nat. Med.* **9**, 448–452 (2003).
62. D. G. Walker, L. F. Lue, Immune phenotypes of microglia in human neurodegenerative disease: Challenges to detecting microglial polarization in human brains. *Alzheimers Res. Ther.* **7**, 56 (2015).
63. P. Yuan *et al*., TREM2 haplodeficiency in mice and humans impairs the microglia barrier function leading to decreased amyloid compaction and severe axonal dystrophy. *Neuron* **90**, 724–739 (2016).
64. R. G. de Rubio *et al*., Phosphatidylinositol 4-phosphate is a major source of GPCR-stimulated phosphoinositide production. *Sci. Signal.* **11**, eaan1210 (2018).
65. M. L. Bennett *et al*., New tools for studying microglia in the mouse and human CNS. *Proc. Natl. Acad. Sci. U.S.A.* **113**, E1738–E1746 (2016).
66. B. Tasic *et al*., Adult mouse cortical cell taxonomy revealed by single cell transcriptomics. *Nat. Neurosci.* **19**, 335–346 (2016).
67. A. Zeisel *et al*., Brain structure. Cell types in the mouse cortex and hippocampus revealed by single-cell RNA-seq. *Science* **347**, 1138–1142 (2015).
68. Y. Ikeda-Matsuo *et al*., Microglia-specific expression of microsomal prostaglandin E2 synthase-1 contributes to lipopolysaccharide-induced prostaglandin E2 production. *J. Neurochem.* **94**, 1546–1558 (2005).
69. T. Maejima *et al*., Synaptically driven endocannabinoid release requires Ca^{2+}-assisted metabotropic glutamate receptor subtype 1 to phospholipase Cbeta4 signaling cascade in the cerebellum. *J. Neurosci.* **25**, 6826–6835 (2005).
70. V. R. Lo Vasco *et al*., Expression of phosphoinositide-specific phospholipase C isoenzymes in cultured astrocytes. *J. Cell. Biochem.* **100**, 952–959 (2007).
71. M. Kawabori *et al*., Triggering receptor expressed on myeloid cells 2 (TREM2) deficiency attenuates phagocytic activities of microglia and exacerbates ischemic damage in experimental stroke. *J. Neurosci.* **35**, 3384–3396 (2015).
72. F. Filipello *et al*., The microglial innate immune receptor TREM2 is required for synapse elimination and normal brain connectivity. *Immunity* **48**, 979–991.e8 (2018).
73. W. J. Meilandt *et al*., Trem2 deletion reduces late-stage amyloid plaque accumulation, elevates the Aβ42:Aβ40 ratio, and exacerbates axonal dystrophy and dendritic spine loss in the PS2APP Alzheimer's mouse model. *J. Neurosci.* **40**, 1956–1974 (2020).
74. E. Maguire *et al*., PIP2 depletion and altered endocytosis caused by expression of Alzheimer's disease-protective variant PLCγ2 R522. *EMBO J.* **40**, e105603 (2021).
75. D. Ogasawara *et al*., Selective blockade of the lyso-PS lipase ABHD12 stimulates immune responses in vivo. *Nat. Chem. Biol.* **14**, 1099–1108 (2018).
76. F. M. Marim, T. N. Silveira, D. S. Lima Jr, D. S. Zamboni, A method for generation of bone marrow-derived macrophages from cryopreserved mouse bone marrow cells. *PLoS One* **5**, e15263 (2010).
77. S. S. Kamat *et al*., Immunomodulatory lysophosphatidylserines are regulated by ABHD16A and ABHD12 interplay. *Nat. Chem. Biol.* **11**, 164–171 (2015).
78. E. V. Vinogradova *et al*., An activity-guided map of electrophile-cysteine interactions in primary human T cells. *Cell* **182**, 1009–1026.e29 (2020).
79. H. Jing, H. Li, B. F. Cravatt, Transcriptome profiles of Plcg2+/+ and Plcg2−/− mouse neonatal microglia. *Gene Expression Omnibus*. https://www.ncbi.nlm.nih.gov/geo/query/acc.cgi?acc=GSE180274. Deposited 16 July 2021.
80. E. W. Deutsch *et al*., The ProteomeXchange consortium in 2017: Supporting the cultural change in proteomics public data deposition. *Nucleic Acids Res.* **45** (D1), D1100–D1106 (2017).
81. H. Jing, A. Reed, H. Li, B. F. Cravatt, PLCG2 regulates endocannabinoid and eicosanoid networks in innate immune cells. PRoteomics IDEntifications Database. https://www.ebi.ac.uk/pride/archive/projects/PXD027350. Deposited 16 July 2021.